



# Modeling of the Fluid Flow and Design of an Experimental Test Stand for Ejector Deep Hole Drilling Processes

J. F. Gerken<sup>1</sup>(✉), D. Biermann<sup>1</sup>, D. Canini<sup>2</sup>, and P. Eberhard<sup>2</sup>

<sup>1</sup> Institute of Machining Technology, TU Dortmund University, Baroper Straße 303, 44227 Dortmund, Germany

julian.gerken@tu-dortmund.de

<sup>2</sup> Institute of Engineering and Computational Mechanics, University of Stuttgart, Pfaffenwaldring 9, 70569 Stuttgart, Germany

**Abstract.** The efficient execution of demanding deep hole drilling operations represents a major challenge for manufacturing companies. The ejector method makes the advantages of deep hole drilling, such as high material removal rate and bore quality, usable for the industry on conventional machining centers. Thus, no expensive deep hole drilling machine with complex sealing system is necessary. The ejector effect is mainly responsible for a stable deep hole drilling process by supplying the working zone with cooling lubricant. In order to realize an enhanced fundamental understanding of the fluid flow in the tool with its process-typical peculiarities, a demanding experimental setup for in-process fluid pressure and volume flow measurement is developed. Based on the results a simulation model is developed with the help of the mesh-free Smoothed Particle Hydrodynamics (SPH) method. The measurements done in the experimental investigations are used as input data for the model generation and the adjustment of the SPH adaptivity.

**Keywords:** Ejector deep hole drilling · Flow of the cooling liquid · Smoothed Particle Hydrodynamics (SPH)

## 1 Introduction

Deep hole drilling methods allow the production of bores with a large bore depth compared to the diameter and they are economically used for a variety of drilling applications with a length-to-diameter-ratio larger than  $l/D > 10$  [1]. The different tool designs are used for the production of deep bores based on specific aspects of the mechanical processes. There are tools with an asymmetrical single-edged design and secondly, there are also tools with two symmetrically arranged cutting edges. Symmetrical tool designs are used in twist and double-lip drilling. The classical deep hole drilling methods with an asymmetrical design are single-lip drilling, ejector drilling with a double-tube system and BTA deep hole drilling with a single-tube system. The asymmetrical design leads to self-centering of the tool in the bore by guide pads [2].

In this paper the ejector deep hole drilling is considered in more detail. The ejector method makes the advantages of deep hole drilling usable for industry on conventional machining centers, since unlike the other deep hole drilling methods no sealings against the cooling lubricant and due to this no special machines are required [3]. Therefore, the optimization of this process is of enormous economic relevance. The current approach in industrial applications is associated with a protracted commissioning of the tool system, which, due to the lack of process knowledge on the ejector effect, is associated with an enormous expenditure of resources. In addition, the required cooling lubricant flow rate is often set higher than necessary during the application, which increases the process costs. The objective of this research work is the deep understanding of the operational behavior of an ejector deep hole drilling system, combining in-process sensor technology and a novel simulation approach, based on the Lagrangian simulation method Smoothed Particle Hydrodynamics (SPH). The data coming from the experimental setup will be the input basis for the simulation model, which will provide a deeper understanding of the peculiarities of the process and of the system, proposing optimization strategies which will then be verified and validated on the experimental rig.

## 2 Process Principle and Tool Design

In contrast to the other deep hole drilling methods ejector tools use differently designed boring bars, onto which the cutting edge section referred to as the “drill head” is screwed. The nominal bore diameter range lies between  $d = 18 \text{ mm}$  to  $65 \text{ mm}$ . Figure 1 shows the typical process principle of ejector deep hole drilling.

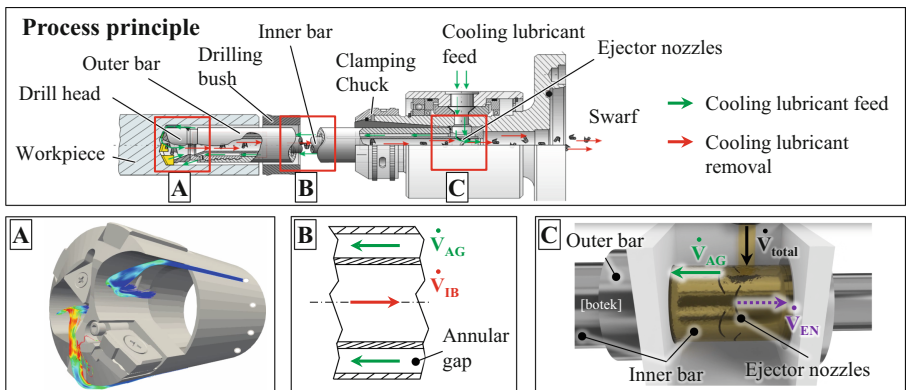


**Fig. 1.** Schematic process principle ejector deep hole drilling; A) Drill head; B) Sectional view of the double tube system; C) Cooling lubricant feed system

The cooling lubricant is fed via a cooling lubricant feed system, which is connected to the main spindle and a high-pressure pump (Fig. 1C). It can be realized with a rotating tool or workpiece. One part of the cooling lubricant with volume flow  $\dot{V}_{AG}$  flows through a second concentrically installed bar into the annular gap between the inner and outer bar (Fig. 1B) and up to the drill head where it emerges through bores, flows around

the cutting edge area and flushes away the chips through the inner bar (Fig. 1A). The chips have no contact with the bore hole wall. Therefore, especially the surface quality is improved [4]. The other part of the cooling lubricant with volume flow  $\dot{V}_{EN}$  flows into through the inner bar via an ejector nozzle to the end of the main spindle. As it flows inside the inner bar, the arrow is marked with a dash line. Thus, a reduction of pressure at the chip mouth is created enabling the return flow of the chip-lubricant-mixture through inner bar. This suction effect, created by the division of the main volume flow  $\dot{V}_{total}$  into  $\dot{V}_{AG}$  and  $\dot{V}_{EN}$ , is creating an ejector effect and is mainly decisive for a stable cutting process. The correlation of the volume flows for a stable drilling process are

$$\dot{V}_{AG} + \dot{V}_{EN} = \dot{V}_{total}, \quad (1)$$

$$\dot{V}_{AG} = \dot{V}_{IB}. \quad (2)$$

Due to this cooling lubricant flow guidance, the inner bar acts like an ejector. Ejectors are jet pumps that aspirate and transport an aspiration medium based on a pressure difference using the Venturi principle with the aid of an accelerated fluid jet [5]. The aspiration of the coolant-chip mixture eliminates the need for a rear seal behind the workpiece. In an unstable process without an ejector effect a leakage occurs and the cooling lubricant sprays into the machine. This means that only in the case of a stable process with ejector effect the condition in Eq. (2) is fulfilled, since the volume flow  $\dot{V}_{AG}$  in the annular gap is equal to the recirculated volume flow  $\dot{V}_{IB}$  in the inner bar. Due to the special boundary conditions of the ejector effect, the application of current methods of flow simulation in close cooperation with production engineering is essential for generating the required knowledge. In order to realize a physically correct simulation of ejector deep hole drilling systems with process-typical peculiarities, a simulation model is to be developed with the help of the mesh-free SPH method.

### 3 Design of the Experimental Test Stand

In order to achieve this goal, an ejector drilling test rig on the INDEX G250 machining center with adapted sensor technology for process analysis is to be designed, see Fig. 2. It allows in-process pressure and volume flow measurements during the deep hole drilling process with a rotating tool. Due to the high technical requirements, such as the fast rotation of the tool ( $n \approx 950 \text{ min}^{-1}$ ) and the resulting high acceleration forces ( $> 30 \text{ g}$ ), the design of the double-tube system (difference in diameter of the annular gap between inner and outer bar  $d_{Diff} = 1 \text{ mm}$ ), and the use in the fully flooded cooling lubricant area, the selection of suitable sensor technology in particular represents a major challenge. The experimental setup with the sensors is shown in Fig. 2. One of the objectives is to determine the volume flow distribution between the ejector nozzles and the annular gap of the two bars, but due to the structure of the ejector system, flow sensors cannot be mounted at these positions. The volume flow rates to be investigated for the bore diameter  $d = 30 \text{ mm}$  are in the range of  $\dot{V}_{total} = 50 \dots 80 \text{ l/min}$ . As a substitute, the supplied volume flow  $\dot{V}_{total}$  into the system and the discharged total volume flows  $\dot{V}_{IB}$  and  $\dot{V}_{EN}$  are determined simultaneously. This not only shows the distribution of the volume flows,

but also the point in time at which the ejector effect begins. The supplied volume flow  $\dot{V}_{\text{total}}$  is always without chips, so a robust mechatronic flow sensor can be used which measuring range and burst pressure correspond to the test parameters. Mechatronic flow sensors measure the velocity of the fluid by measuring the displacement of a pin which is located at a  $45^\circ$  angle to the flow direction. Because of the chips, a non-contact measuring method is required for the discharged volume flow. Due to this, contact-free magnetic inductive sensors are used in which a magnetic field is generated in the bar cross-section at  $90^\circ$  angles to the flow direction.

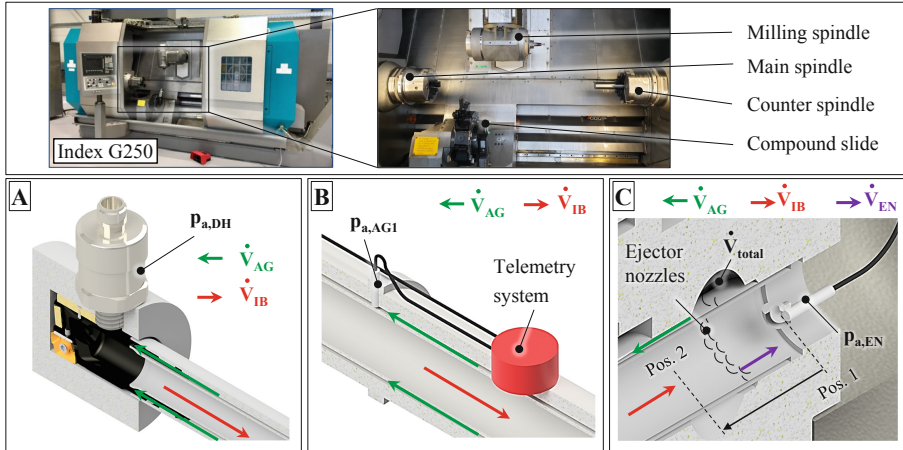


**Fig. 2.** Adapted sensor system for static absolute pressure measurement on the ejector deep hole drilling system (drilling diameter  $d = 30$  mm), A) Pressure measurement in range of the drill head outlets B) Pressure measurement in the annular gap C) Pressure measurement in front (pos. 1) and behind (pos. 2) the ejector nozzles in the inner bar

The fluid flowing through the tube induces a current on the pipe wall, of which the voltage is linearly related to the flow velocity [6]. This method requires a fluid with an electrical conductivity of at least  $20 \mu\text{S}/\text{cm}$ , which applies to the used emulsion of water and the esteril-based cooling lubricant.

The pressure sensors are subject to the same conditions as the flow sensors. The resulting pressures in the system depend on the sensor position. Pressures in the range of  $p = 10 \dots 20$  bar are expected in the overall system. To measure the pressure  $p_{a,AG}$  in the annular gap between the inner and outer bar, the sensor must be radially fixed to the outer bar (Fig. 2B). The challenge of radial mounting of the pressure sensors are the high acceleration forces, which occur at  $950 \text{ min}^{-1}$  and the data transmission of the rotating sensors. The first consideration to use wireless sensors had to be discarded, because the dimensioning of common wireless sensors does not withstand the permanent use under fast rotation. Instead, miniature wired sensors by Kulite in combination with a Datatel telemetry system were selected. The sensors short length of  $9.5 \text{ mm}$  minimizes the acceleration forces orthogonal to the measuring cell. Furthermore, due to the original field of application in turbomachinery, the manufacturer provides the measurement

deviation as a function of acceleration forces, which allows a correct measurement of the pressure under radial installation. The encapsulated design also allows the use of this sensor for pressure measurement in the flooded inner bar (Fig. 2C). This requires the use of absolute pressure sensors, as no permanent contact with the ambient atmosphere can be guaranteed at this position [7]. With the help of an additively manufactured holder, the positioning of sensor  $p_{a,EN}$  is variable. It can be positioned behind (position 1) and in front of (position 2) the ejector nozzles in the inner bar. Because of the non-rotating workpiece, standard pressure sensors can be used for the measurement in range of the drill head outlets (Fig. 2A). To make all measurements consistent, these are used in the variant which also measures the absolute pressure.

## 4 Simulation Environment

### 4.1 Smoothed Particle Hydrodynamics

The simulations in this project are performed applying the Lagrangian smoothed particle hydrodynamics (SPH) method, which uses interpolation points, commonly called particles, moving along with the continuum. Applying this method to a set of partial differential equations (PDE) converts them into ordinary differential equations (ODE) in time, solvable with common time integration schemes [8].

*Applied SPH formulation.* The weakly compressible SPH is applied to solve the Navier-Stokes equations, that in Lagrangian form are

$$\frac{d\rho}{dt} = -\rho \nabla \cdot \mathbf{v}, \quad (3)$$

$$\frac{d\mathbf{v}}{dt} = \frac{1}{\rho} \left( -\nabla p + \mu \nabla^2 \mathbf{v} + \mathbf{f} + \nabla \mathbf{R} \right), \quad (4)$$

$$\frac{d\mathbf{r}}{dt} = \mathbf{v} \quad (5)$$

with  $\rho$  being the density,  $p$  the pressure,  $\mu$  the dynamic viscosity,  $\mathbf{r}$  the position,  $\mathbf{v}$  the velocity,  $\mathbf{f}$  the external forces, and  $\mathbf{R}$  the Reynolds turbulent stresses. As seen in Eq. (3) the fluid is not modeled incompressible: it allows a small fluctuation of the density.

An almost incompressible behavior is obtained applying an equation of state, relating density and pressure, which restores a force which operates against the concentration of the fluid. In this work, the isothermal equation of state presented in [9] is applied

$$p = \frac{\rho_0 c_0^2}{\gamma} \left[ \left( \frac{\rho}{\rho_0} \right)^\gamma - 1 \right] + p_B \quad (6)$$

in which  $\rho_0$  is the reference density,  $p_B$  the background pressure and the exponent  $\gamma$  is a scaling factor usually equal to 7 for water. The speed of sound  $c_0$ , according to [8], is set to be 10 times faster than the maximum expected velocity, in such a way that density fluctuations are limited to be less than 1%. The SPH method transforms

the Navier-Stokes equations in a set of ODE. The conservation of mass in Eq. (5), as example, calculated summing over all the neighboring particles is

$$\frac{d\rho_a}{dt} = -\rho_a \sum_b \frac{m_b}{\rho_b} \mathbf{v}_{ab} \cdot \nabla_a W_{ab}, \quad (7)$$

where  $\rho_a$  and  $\rho_b$  are, respectively, the densities of particles a and b,  $m_b$  is the mass of the particles,  $\mathbf{v}_{ab} = \mathbf{v}_a - \mathbf{v}_b$  is the relative velocity and the term  $\nabla_a W_{ab}$  is the gradient of the SPH kernel function, calculated with respect to the coordinates of particle a. The SPH kernel function, also called smoothing function, regulates the interaction between different particles. In this work, the Wendland kernel function [10] is used

$$W(\mathbf{r}_{ab}, h) = \alpha_D \left(1 - \frac{|\mathbf{r}_{ab}|}{2h}\right)^4 \left(2 \frac{|\mathbf{r}_{ab}|}{h} + 1\right), \quad \text{for } 0 \leq \frac{|\mathbf{r}_{ab}|}{h} \leq 2 \quad (8)$$

with  $\alpha_D = 21/(16\pi h^3)$ . The pressure term in Eq. (4) can be approximated as:

$$\nabla p_a = \rho_a \sum_b m_b \left( \frac{p_a}{\rho_a^2} + \frac{p_b}{\rho_b^2} \right) \nabla_a W_{ab} \quad (9)$$

with  $p_a$  and  $p_b$  being the pressures of particle a and b, while the viscous term is calculated, according to [11] as

$$\mu_a \nabla^2 \mathbf{v}_a = \rho_a \sum_b \frac{m_b (\mu_a + \mu_b) \mathbf{r}_{ab} \cdot \nabla_a W_{ab}}{\rho_a \rho_b (\|\mathbf{r}_{ab}^2\| + 0.01h^2)} \mathbf{v}_{ab} \quad (10)$$

where  $\mathbf{v}_a$  is the velocity of particle a,  $h$  the SPH smoothing length,  $\mathbf{r}_{ab}$  the distance between particle a and b,  $\mu_a$  and  $\mu_b$  the dynamic viscosities of particles a and b.

An artificial viscosity term is then applied to stabilize the simulations. In accordance with [12], this term reads

$$\Pi_{ab} = \begin{cases} \frac{-\alpha \bar{c}_{ab} \mu_{ab} + \beta \mu_{ab}^2}{\bar{\rho}_{ab}}, & \text{if } \mathbf{v}_{ab} \cdot \mathbf{r}_{ab} < 0, \\ 0, & \text{otherwise} \end{cases} \quad (11)$$

with the average density  $\bar{\rho}_{ab} = (\rho_a + \rho_b)/2$ , the average sound velocity  $\bar{c}_{ab} = (c_a + c_b)/2$ , and the artificial viscosity

$$\mu_{ab} = \frac{h \mathbf{v}_{ab} \cdot \mathbf{r}_{ab}}{\|\mathbf{r}_{ab}^2\| + 0.01h^2}. \quad (12)$$

The parameters  $\alpha$  and  $\beta$  are usually chosen close to the value 1 for  $\alpha$  and 2 for  $\beta$ . An explicit second order predictor-corrector leapfrog integrator is applied, whose time step size is controlled by the Courant-Friedrichs-Lewy (CFL) conditions

$$\Delta t_{CFL} = \alpha \frac{h}{c_s}. \quad (13)$$

*Boundaries.* To describe SPH boundaries for arbitrarily shaped boundaries, triangular meshes coupled with SPH particles by the Lennard-Jones penalty approach, as proposed in [13], are used. Being  $d$  the distance between the interacting particle and the triangle and  $R$  the maximum distance for which contact occurs, the resulting force  $F$  acting on the triangle's normal direction is

$$F(d) = \begin{cases} \psi \frac{(R-d)^4 - (R-s)^2(R-d)^2}{R^2 s(2R-s)}, & \text{if } d \leq R, \\ 0, & \text{otherwise} \end{cases} \quad (14)$$

The parameter  $s$  denotes the distance for which the force  $F(d)$  switches from repulsive to attractive, while the scalar  $\psi$  indicates the maximum force at zero distance, i.e.,  $F(0) = \psi$ .

*Pasimodo.* To perform the simulations the software Pasimodo [14] is used. Developed at the Institute of Engineering and Computational Mechanics since more than a decade and involved in many different projects, it offers a plugin-based framework for general particle methods. The software is written in a highly object oriented environment and consists of a core and multiple plugins. The core, independent of the specific particle method applied, controls the basic steps necessary for any method: firstly, the neighbor search step, detecting the interacting particles, then the interaction step, calculating the interaction forces, and lastly the integration step, moving the particles according to the interaction calculated in the previous step. The plugins, on the other hand, are compiled as shared libraries which are dynamically loaded and can be programmed or modified without full knowledge of the core. They are used to implement specific methods and algorithms.

## 4.2 Modelling and Simulation of Drilling System

The transient motion of the cooling lubricant at the cutting area is investigated. The drill considered has external diameter  $\phi_{ext} = 30$  mm, the inflow velocity is set, considering the standard flow rate of application, to be  $v_{in} = 11,4$  m/s, the particles are created in a Cartesian pattern with initial distance  $x_{dist} = 4 \cdot 10^{-4}$  m and smoothing length  $h = 6 \cdot 10^{-4}$  m for a total of about 600000 particles. The Courant-Friedrich-Lewy (CFL) condition controls the time step size, which in average results to be  $\Delta t_{AV} = 5.46 \cdot 10^{-8}$  s for 0.01 s of the SPH simulation. Figure 3 and 4 show the flow evolution in time, respectively from the internal and external view, with respect to the drill head.

The simulation considers, as a first approximation, a laminar flow approaching the cutting area. No problematic effects around the guide strips and the cutting edges are detectable. The flow is not excessively disturbed by the presence of this components and does not present counterproductive tendencies to trigger extremely turbulent motions. This behavior is crucial to ensure the stability of the flow in the whole system and the effectiveness of the ejector effect. The stability of the flow and of the ejector effect during the exercise is fundamental for the adequate cooling of the drill and for the removal of the material while minimizing the quantity of fluid needed for the operation.

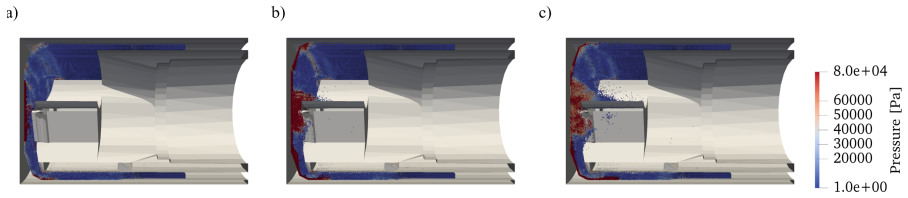


**Fig. 3.** Transient evolution at the cutting edge, internal view. Evolution time: a)  $t = 0.008$  s; b)  $t = 0.009$  s; c)  $t = 0.01$  s.

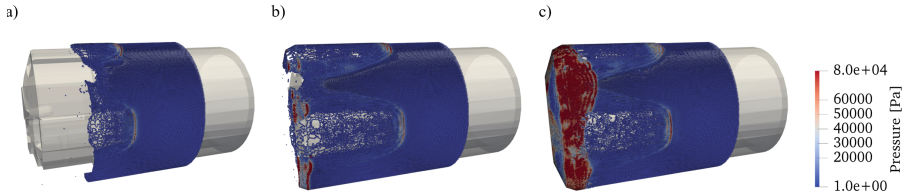


**Fig. 4.** Transient evolution at the cutting edge, external view. Evolution time: a)  $t = 0.004$  s; b)  $t = 0.006$  s; c)  $t = 0.008$  s.

## 5 Conclusion and Outlook

In this paper, an experimental test rig was designed to enable in-process pressure and volume flow measurement in ejector deep hole drilling with a rotating tool. For a realistic representation of the physical conditions when the ejector effect occurs, knowledge of the pressure and volume flow conditions at the positions worked out is indispensable. More in-depth investigations are carried out to gain a physical understanding of the correlations in the development of the ejector. In current studies, a calibrated pressure is applied to the sensors on a reference test stand and determined both with and without rotation using the Kulite's sensors and a reference barometer. In addition, the test rig will be extended by components of the ejector deep hole drilling system made of acrylic glass, so that the visualization of the flow using tracer particles for the detailed analysis. The simulations, using the data from the test setup as input, will provide a better understanding of the system behavior, focusing on the three areas of major interest: the cutting area, the inflow area and the ejector nozzles. Based on the resulting deeper process understanding of the behavior of the coolant during ejector deep hole drilling, new optimization strategies for increasing deep hole drilling efficiency will be developed.

**Acknowledgments.** Funded by the Deutsche Forschungsgemeinschaft (German Research Foundation). Gefördert durch die Deutsche Forschungsgemeinschaft (DFG) – Projektnummer 439917965.

## References

1. Biermann, D., Bleicher, F., Heisel, U., Klocke, F., Möhring, H.C., Shih, A.: Deep hole drilling. CIRP Ann. **67**, 673–694 (2018)



2. Hagemeyer, C.: Stütz- und Führungsleistennormalkräfte beim BTA-Aufbohren. WGP-Bericht, pp. 38–43 (1990)
3. Katsuki, A., Sakuma, K., Tabuchi, K., Onikura, H., Akiyoshi, H., Nakamuta, Y.: The influence of tool geometry on axial hole deviation in deep drilling: comparison of single- and multi-edge tools. *JSME Int. J.* **30**(265), 1167–1174 (1987)
4. VDI-Richtlinie: 3209: Tiefbohren mit äußerer Zuführung des Kühlschmierstoffes (BTA- und ähnliche Verfahren). VDI-Gesellschaft Produktion und Logistik (1999)
5. Grazzini, G., Milazzo, A., Mazzelli, F.: *Ejectors for Efficient Refrigeration*. Springer, Heidelberg (2018). <https://doi.org/10.1007/978-3-319-75244-0>
6. Krause, J., Stange, G.: Magnetic-inductive flow sensor with variable cross section – design using FEA. *tm -Technisches Messen* **74** Heft 6, (2007)
7. Hesse, S., Schnell, G.: *Sensoren für die Prozess- und Fabrikautomation*. Springer, Wiesbaden (2018). <https://doi.org/10.1007/978-3-658-05867-8>
8. Monaghan, J.J.: Smoothed particle hydrodynamics. *Rep. Prog. Phys.* **68**(8), 1703 (2005)
9. Murnaghan, F.D.: The compressibility of media under extreme pressures. *Proc. Natl. Acad. Sci. U.S.A.* **30**(9), 244 (1944)
10. Wendland, H.: Piecewise polynomial, positive definite and compactly supported radial functions of minimal degree. *Adv. Comput. Math.* **4**(1), 389–396 (1995)
11. Morris, J.P., Fox, P.J., Zhu, Y.: Modeling low reynolds number incompressible flows using SPH. *J. Comput. Phys.* **136**(1), 214–226 (1997)
12. Monaghan, J.J.: Smoothed particle hydrodynamics. *Ann. Rev. Astron. Astrophys.* **30**(1), 543–574 (1992)
13. Monaghan, J.J.: Simulating free surface flows with SPH. *J. Comput. Phys.* **110**(2), 399–406 (1994)
14. Pasimodo: <https://www.itm.uni-stuttgart.de/software/pasimodo/>. Accessed 14 April 2021